Front. Chem. China 2007, 2(3): 303–306
DOI 10.1007/s11458-007-0055-z

RESEARCH ARTICLE

YUAN Zhengyong, YUAN Liangjie, SUN Jutang

Synthesis and properties of nanosized tin-zinc composite oxides as lithium storage materials

Abstract After preparing the precursor by a liquid precipitation method, a series of tin-zinc composite oxides with different components and structures were synthesized as the anode materials for lithium ion batteries when the precursor was pyrolyzed at different temperatures. The products were characterized by X-ray diffraction (XRD), transmission electron microscopy (TEM), and electrochemical measurements. The reversible capacity of amorphous $ZnSnO_3$ is 844 mA·h/g in the first cycle and the charge capacity is 695 mA·h/g in the tenth cycle. The reversible capacity of $ZnO \cdot SnO_2$ is 845 mA·h/g in the first cycle and the charge capacity is 508 mA·h/g in the tenth cycle. The reversible capacity of $SnO_2 \cdot Zn_2SnO_4$ is 758 mA·h/g in the first cycle and the charge capacity is 455 mA·h/g in the tenth cycle. Results show that amorphous $ZnSnO_3$ exhibits the best electrochemical property among all of the tin-zinc composite oxides. With the formation of crystallites in the samples, the electrochemical property of the tin-zinc composite oxides decreases.

Keywords tin-zinc composite oxides, lithium ion battery, lithium storage materials

1 Introduction

Recently, the amorphous tin-based oxides as lithium storage materials have received considerable attention as promising new negative-electrode material for lithium ion batteries due to their high volumetric and gravimetric capacity [1−6]. Courtney and Dahn [7] claimed that the reaction of tin oxides with lithium proceeds in two steeps. Initially, the tin oxides are reduced by lithium to form a small cluster of tin metal, and dispersed in Li_2O framework. Further, lithium can be reversibly inserted into metallic tin to form Li/Sn alloy. Lithium inserts into the metallic tin directly to cause a large volume expansion. The expansion and subsequent contraction on removal of lithium cause disintegration of the structure, and cause rapid loss of capacity and rechargeability. The use of amorphous Li_2O or other inactive materials as a matrix can constrain the volume expansion and contraction during cycling [8,9]. Prior works [3,10] have shown that both decreasing the particle size and preparing tin-based oxide with amorphous structure are favorable to increase the capacity and life cycle.

Zinc oxide is another promising negative-electrode material for lithium-ion batteries because it can also form an alloy with lithium as tin. Prior works [11,12] have shown that the reaction mechanism of ZnO with Li^+ was the same as the tin oxides. ZnO is reduced to form zinc metal and dispersed in Li_2O framework in the first cycle when cycled over a voltage window of 0−2.0 V versus Li^+/Li. This is an irreversible process. Lithium can be inserted into the metallic zinc to form Li_2Zn_5, $LiZn_2$, Li_2Zn_3, and LiZn alloy with the voltage decrease, and reversibly removed in the charge process. Tin-zinc composite oxides have received considerable attention for their application as active materials of transducer for the gases which are flammable, blasting or poisonous such as H_2, CH_4, C_2H_6, C_2H_5OH, CO, NO, and NO_2, etc. Belliard et al. [13,14] reported tin-zinc composite oxides synthesized by ball mill and solid state reaction at high temperature, and electrochemical performances as negative electrode material for lithium-ion batteries were investigated. However, the reversible capacities were between 400 and 600 mA·h/g and cycling performance was poor.

In this paper, a series of tin-zinc composite oxides as negative-electrode materials for lithium-ion batteries are reported. The precursor was prepared with liquid precipitation method. A series of tin-zinc composite oxides with different components and structures were synthesized when

Translated from *Chem J Chin Univ*, 2006, 27(12): 2252–2255 [译自: 高等学校化学学报]

YUAN Zhengyong, YUAN Liangjie, SUN Jutang (✉)
College of Chemistry and Molecular Science, Wuhan 430072, China
E-mail: jtsun@whu.edu.cn

YUAN Zhengyong
Ningbo Free Trade Zone Postdoctoral Workstation, Ningbo 315800, China
Ningbo Best Winning Technology Limited Company, Ningbo 315800, China

the precursor was pyrolyzed at different temperatures, and the electrochemical properties of tin-zinc composite oxides were investigated.

2 Experimental

Preparation of samples: Na_2SnO_3 and $ZnSO_4$ are of analytical reagent grade. Stoichiometric Na_2SnO_3 and $ZnSO_4$ solution were mixed under continuous stirring and precipitation occurred instantly. The white precipitate obtained was washed with distilled water to remove SO_4^{2-}, and finally dried in an oven at 120°C to get the $ZnSn(OH)_6$ precursor. The precursor was pyrolyzed at different temperatures to form tin-zinc composite oxides with different components and structures.

Thermogravimetric and differential thermal analysis (TG/DTA) were performed using Shimadzu DT-40 thermal analyzer at a heating rate of 10°C min^{-1} in air. X-ray diffraction (XRD) was conducted on a Shimadzu XRD-6000 diffractometer (Cu $K\alpha_1$ radiation) to reveal the structural evolution. Transmission electron microscopic (TEM) images were obtained with a Joel JEM–100CXII microscope. Electrochemical tests were performed using Neware battery testing system.

Working electrodes were prepared by pressing a film composed of tin-zinc composite oxide powders, acetylene black and polytetrafluoroethylene binder (weight ratio of 6:3:1) onto a stainless steel current collector. The cells were discharged and charged between 0 and 2.0 V vs Li^+/Li at a constant current of 50 mA g^{-1}.

3 Results and discussion

3.1 TG and DTA curves of the precursor

Figure 1 shows the DTA and TG curves of the $ZnSn(OH)_6$ precursor. The endothermic peak located at about 220°C corresponds to a weight loss of 18.5% that can be noticed on the curves between 150°C and 280°C. This is attributed to the decomposition of the $ZnSn(OH)_6$ precursor to form $ZnSnO_3$.

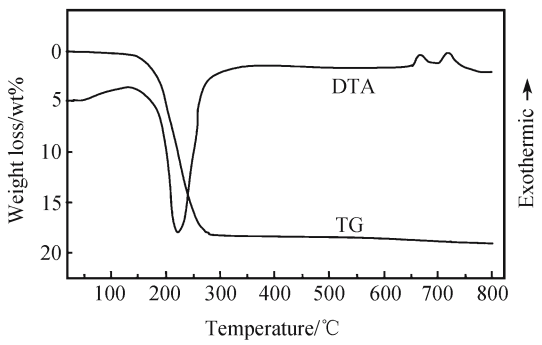

Fig. 1 TG and DTA curves of $ZnSn(OH)_6$ in air

The observed weight loss is almost consistent with the theoretical weight loss of 18.89%. Two small exothermic peaks located at 670°C and 720°C on the DTA curve can be attributed to the crystallization at high temperature and the forming reaction of $ZnSnO_3$.

3.2 XRD patterns

Figure 2(a) shows the XRD patterns of the $ZnSn(OH)_6$ precursor. It confirms that the precursor is $ZnSn(OH)_6$ without any impurity phases. The XRD data correspond with the JCPDS card no. 20–1455. Figure 2(b) shows the XRD patterns of the $ZnSnO_3$ synthesized by means of the pyrolysis of the precursor $ZnSn(OH)_6$ at 300°C for 6 h. For the product, no diffraction peaks can be observed in Fig. 2(b). This indicates that the structure of $ZnSnO_3$ is amorphous or amorphous-like. Several broad diffraction peaks in Fig. 2(c) can be observed for the sample synthesized by means of the pyrolysis of the precursor $ZnSn(OH)_6$ at 670°C for 6 h. This indicates that new crystalline forms at this temperature. These diffraction peaks are the characteristic peaks of SnO_2. It implies that the small exothermic peak located at 670°C on the DTA curve is attributed to the crystallization of the SnO_2. The average size of the particles is 4.8 nm calculated through Scherrer formula. No diffraction peaks of ZnO and Zn–Sn composite oxides are observed. It indicates that the structure of Zn–Sn composite oxides is amorphous. Fig. 2(d) shows the XRD patterns of the sample synthesized by means of the pyrolysis of the precursor $ZnSn(OH)_6$ at 800°C for 6 h. The small exothermic peak located at 720°C on the DTA curve can be attributed to the reaction of SnO_2 and ZnO to produce Zn_2SnO_4. The average sizes of the particles of SnO_2 and Zn_2SnO_4 are 5.5 and 10.5 nm calculated through Scherrer formula, respectively.

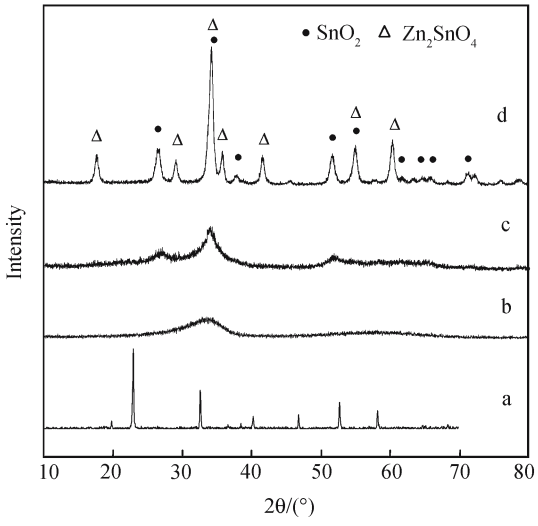

Fig. 2 XRD patterns for precursor (a) $ZnSn(OH)_6$; (b) $ZnSnO_3$; (c) $ZnO \cdot SnO_2$; and (d) $SnO_2 \cdot Zn_2SnO_4$

3.3 TEM images

Figure 3 shows the TEM images of the $ZnSn(OH)_6$ sample heat-treated at different temperatures. The TEM image of $ZnSn(OH)_6$ is shown in Fig. 3(a). The average size of the particles is 70 nm with the square shape, and the particles disperse well. The TEM image of $ZnSnO_3$ obtained from heat-treating precursor is shown in Fig. 3(b). The average size of particles is 70 nm with the square shape, and the particles disperse well. Although the $ZnSnO_3$ sample is amorphous, the shape and size of particles do not change with the structure of the sample, and is the same as the sample of $ZnSn(OH)_6$ The needed size and shape of the composite materials can be prepared by controlling the size and shape of precursor particles. The TEM image of $ZnO \cdot SnO_2$ obtained by means of the pyrolysis of the precursor $ZnSn(OH)_6$ at 670°C is shown in Fig. 3(c). The average size of particles is 70 nm with the same shape as the precursor. Figure 3(d) shows the TEM image of the $SnO_2 \cdot Zn_2SnO_4$ sample synthesized by means of pyrolyzing $ZnSn(OH)_6$ at 800°C. The particle structure of the $ZnSn(OH)_6$ is destroyed at high temperature to produce some small irregular particles.

3.4 Discharge-charge profile of test cells

Figure 4 shows the initial two discharge-charge curves of the $ZnSn(OH)_6$ sample heat-treated at different temperature. In the first discharge curve of the amorphous $ZnSn(OH)_6$, two plateaus at about 1.1 and 0.65 V can be observed (Fig. 4(a)). The discharge capacity reaches 1 951 mAh g^{-1} and the charge capacity is 844 mAh g^{-1} in the first cycle. The first-cycle irreversible loss was 54.8%. Fig. 4(b) shows the initial two discharge-charge curves of the $ZnO \cdot SnO_2$ sample. In the first discharge curve, a plateau at about 1.1 V can be observed. The discharge capacity reaches 1 700 mAh g^{-1} and the charge capacity is 845 mAh g^{-1} in the first cycle. The first-cycle irreversible loss was 50%. Fig. 4(c) shows the initial two discharge-charge curves of the $SnO_2 \cdot Zn_2SnO_4$ sample. In the first discharge curve, two plateaus at about 0.94 and 0.5V can be observed. The voltage level of the first plateau matches with the reduction of SnO_2, and the second plateau matches with the reduction of Zn_2SnO_4. The discharge capacity reaches 1 497 mAh g^{-1} and the charge capacity 758 mAh g^{-1} in the first cycle. The first-cycle irreversible loss was 49%.

3.5 Cycling performance

The cycling behavior of sample heat-treated $ZnSn(OH)_6$ at different temperatures within ten cycles is shown in Fig. 5. To help quantify the cycling stability of the different samples, a parameter called the capacity retention index is defined. The parameter $R_{10/1}$ is the capacity in the tenth charge cycle divided by the capacity in the first cycle. It can be seen from Fig. 5(a) that the charge capacity is 695 mAh g^{-1} after the tenth discharge-charge cycles, $R_{10/1} = 82.3\%$. The cycling behavior of $ZnO \cdot SnO_2$ sample within ten cycles is shown in Fig. 5(b). The charge capacity is 508 mAh g^{-1} after the tenth discharge-charge cycles, $R_{10/1} = 60.1\%$. The performance of $ZnSnO_3$ as lithium storage is better than that of $ZnO \cdot SnO_2$. The cycling behavior of $SnO_2 \cdot Zn_2SnO_4$ sample within ten cycles is shown in Fig. 5(c). The charge capacity is 455 mAh g^{-1} after the tenth discharge-charge cycles, $R_{10/1} = 60.0\%$.

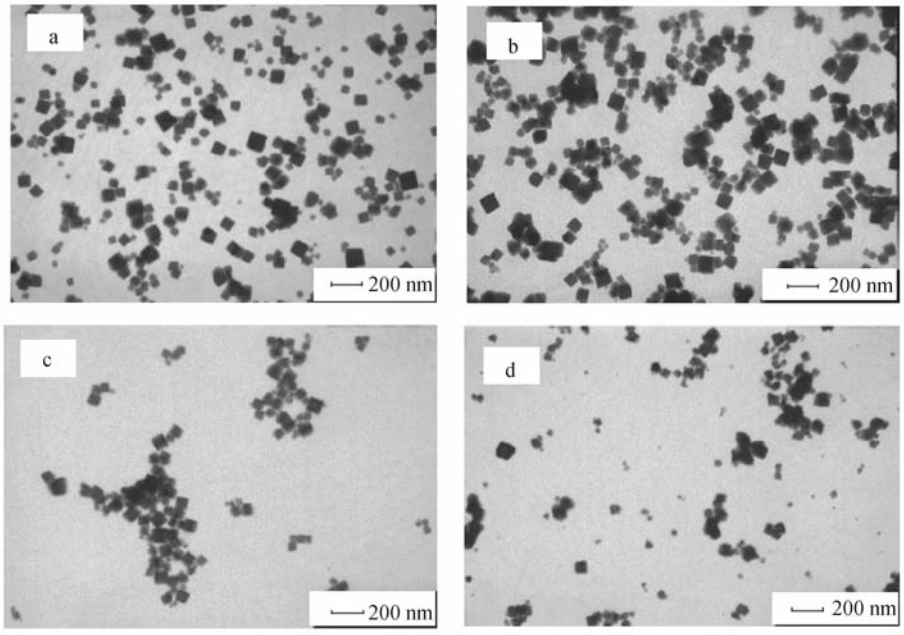

Fig. 3 TEM images for precursor (a) $ZnSn(OH)_6$; (b) $ZnSnO_3$; (c) $ZnO \cdot SnO_2$; and (d) $SnO_2 \cdot Zn_2SnO_4$

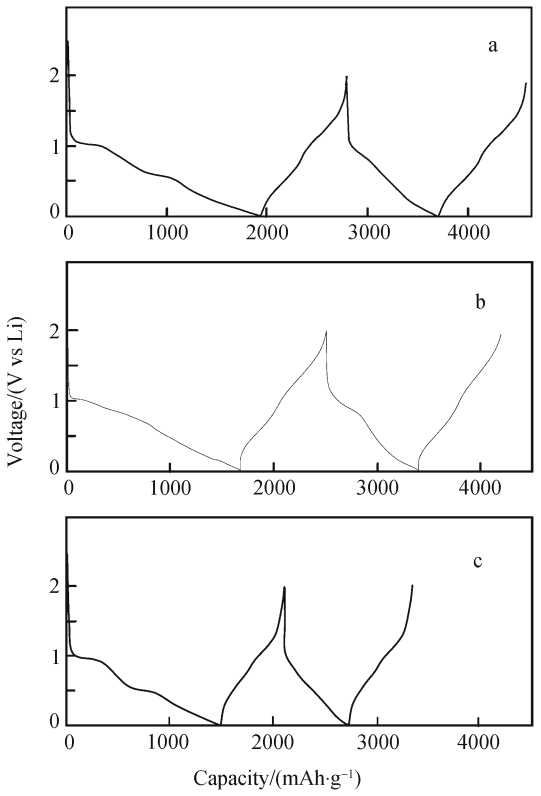

Fig. 4 The first two cycle curves of (a) $ZnSnO_3$/Li test cell; (b) $ZnO \cdot SnO_2$/Li test cell; and (c) $SnO_2 \cdot Zn_2SnO_4$/Li test cell

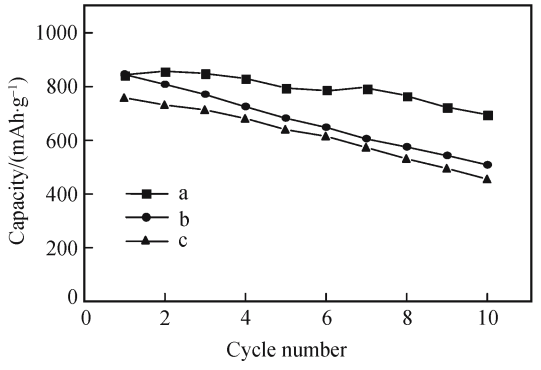

Fig. 5 Cycle-ability of test cells (a) $ZnSnO_3$/Li; (b) $ZnO \cdot SnO_2$/Li; and (c)$SnO_2 \cdot Zn_2SnO_4$/Li

4 Conclusions

The $ZnSn(OH)_6$ precursor was prepared using liquid precipitation method. The precursor was pyrolyzed at different temperatures to form tin-zinc composite oxides with different components and structures. The tin-zinc composite oxides show high capacity and excellent cycle-ability. Amorphous $ZnSnO_3$ exhibits the best electrochemical property among all of the tin-zinc composite oxides. The reversible capacity is 844 mAh g^{-1} in the first cycle and the charge capacity is 695 mAh g^{-1} in the tenth cycle. The reversible capacity of $ZnO \cdot SnO_2$ is 845 mAh g^{-1} in the first cycle and the charge capacity is 508 mAh g^{-1} in the tenth cycle. The reversible capacity of $SnO_2 \cdot Zn_2SnO_4$ is 758 mAh g^{-1} in the first cycle and the charge capacity is 455 mAh g^{-1} in the tenth cycle. The electrochemical property of tin-zinc composite oxides decreases with the formation of crystallites.

Acknowledgements This work was supported by the National Natural Science Foundation of China (Grant No. 20471044).

References

1. Idota Y, Kubota T, Matsufuji A, Maekawa Y, Miyasaka, T. Tin-based amorphous oxide: A High-Capacity Lithium-Ion–Storage Material. Science, 1997, 276: 1395–1397
2. Yuan Z Y, Huang F, Sun J T, Zhou Y H. An amorphous nanosized tin-zinc composite oxide as a high capacity anode material for lithium ion batteries. Chem Lett, 2002, (3): 408–409
3. Mohamedi M, Lee Seo-Jae, Takahashi D, Nishizawa M, Itoh T, Uchida I. Amorphous tin oxide films: preparation and characterization as an anode active material for lithium ion batteries. Electrochim Acta, 2001, 46(8): 1161–1168
4. Chouvin J, Vicente C P, Olivier-Fourcade J, Jumas J-C, Simon B, Biensan P. Deeper insight on the lithium reaction mechanism with amorphous tin composite oxides. Solid State Sci, 2004, 6(1): 39–46
5. Hatchard T D, Dahn J R. Study of the electrochemical performance of sputtered $Si_{1-x}Sn_x$ Films. J Electrochem Soc, 2004, 151(10): A1628–A1635
6. Choi W, Lee J Y, Jung B H, Lim H S. Microstructure and electrochemical properties of a nanometer-scale tin anode for lithium secondary batteries. J Power Sources, 2004, 136(1): 154–159
7. Courtney I A, Dahn J R. Electrochemical and in situ X-Ray diffraction studies of the reaction of lithium with tin oxide composites. J Electrochem Soc, 1997, 144(6): 2045–2052
8. Courtney I A, McKinnon W R, Dahn J R. On the aggregation of tin in Sno composite glasses caused by the reversible reaction with lithium. J Electrochem Soc, 1999, 146(1): 59–68
9. Li H, Huang X J, Chen L Q. Electrochemical impedance spectroscopy study of SnO and Nano-SnO anodes in lithium rechargeable batteries. J Power Sources, 1999, 81–82: 340–345
10. Li Naichao, Martin C R. A High-Rate, High-Capacity, Nanostructured Sn-Based anode prepared using Sol-Gel template synthesis. J Electrochem Soc, 2001, 148(2): A164-A170
11. Li H, Huang X J, Chen L Q. Anodes based on oxide materials for lithium rechargeable batteries. Solid State Ionics, 1999, 123: 189–197
12. Belliard F, Irvine J T S. Electrochemical performance of ball-milled ZnO–SnO_2 systems as anodes in lithium-ion battery. J Power Sources, 2001, 97–98: 219–222
13. Belliard F, Connor P A, Irvine J T S. Novel tin oxide-based anodes for Li-Ion batteries. Solid State Ionics, 2000, 135: 163–167
14. Connor P A, Irvine J T S. Novel tin oxide spinel-based anodes for Li-Ion batteries. J Power Sources, 2001, 97–98: 223–225